State University of Campinas

Gleb Wataghin Institute of Physics

Department of Cosmic Rays and Chronology

MONOGRAPHY

Study of elliptic flow and simulation techniques in ultrarelativistic heavy-ion collisions

Luiza Lober de Souza Piva

llober@ifi.unicamp.br

Advisor: David Dobrigkeit Chinellato

daviddc@ifi.unicamp.br

Department of Cosmic Rays and Chronology

Gleb Wataghin Institute of Physics

Campinas - São Paulo

November, 2019

"The world is indeed full of peril, and in it there are many dark places; but still there is much that is fair, and though in all lands love is now mingled with grief, it grows perhaps the greater".

J.R.R. Tolkien, *The Fellowship of the Ring*

Acknowledgements

I would like firstly to express my thanks to my advisor, Prof. Dr. David Dobrigkeit Chinellato, for his essential role in the undergraduate project that introduced me to the high-energy field, for his patience, great dedication and for all of the discussions we've had throughout this work.

I'm thankful for all of the great feedback and physics discussions that I've had with the HadrEx members, in special Willian Serenone, André Vieira da Silva, Mauricio Hippert, Gabriel Reis Garcia and João Barbon.

Also, I would like to thank all of the fantastic people that I've met through my graduation and that have become closer friends, some of them having a direct or indirect contribution to this work, namely Gabriel Aller Tolentino Oliveira, Letícia Fernandes Soriani, Maria Paula Orfanelli, Matheus Loures, Ana Elisa Barioni, Maira Barbara and João Victor Ramalho Reis.

And, most of all, I would like to thank my family, particularly Luciane Lober de Souza, my mother, and Jayr Piva Júnior, my father, for always supporting my wish to become a physicist and making this journey possible.

Abstract

The extreme conditions obtained when colliding ultra-relativistic heavy-ions at modern particle accelerators lead to the predicted formation of strongly interacting matter, where phenomena such as assymptotic freedom, become relevant. This state of matter, as an analogy to the electronic plasma, is called a Quark-Gluon Plasma (QGP), and observing evidence of its existence is a goal to experiments such as the ALICE collaboration at the LHC. A full theoretical description of the systems created in such collisions is an open challenge in the field of high-energy nuclear physics, and given this difficulty, the most common description treats the various stages of the system's evolution through different models for each step of the collision process. In these models, the system undergoes a QGP phase simulated using relativistic hydrodynamics and, after a expansion and cool-down phase, it then hadronizes via sampling of the energy-momentum hypersurface. The resulting hadrons are then still left to interact both elastically and inelastically in a hadronic phase simulated using hadron cascade models, until hadron densities are low enough that no further interactions will occur. Because such models utilize several physical assumptions and components to calculate final-state hadrons, they are called *hybrid models*.

In this work, we propose to study the elliptic flow v_2 of charged particles created in Pb-Pb collisions at the energies of $\sqrt{s_{\rm NN}} = 2.76$ TeV using a hybrid model that employs the MUSIC hydrodynamic simulator as well as UrQMD to emulate the hadronic phase. This final-state v_2 will be compared to initial state conditions as well as to available experimental data from the ALICE experiment at these same energies.

Keywords: heavy-ion collisions, phenomenology, quark-gluon plasma.

Resumo

As condições extremas obtidas em colisões ultrarrelativísticas de íons pesados em aceleradores de partículas modernos levam à formação de um estado de matéria altamente interagente, onde fenômenos como a liberdade assintótica, se tornam relevantes. Esse estado da matéria, em analogia ao plasma de elétrons, é chamado de Plasma de Quarks e Glúons (QGP, sigla em inglês para *Quark-Gluon Plasma*), e observar evidências de sua existência é um dos objetivos de experimentos com os da colaboração ALICE, no LHC. Uma descrição teórica completa dos sistemas criados em tais colisões é um desafio em aberto na área de física nuclear de altas energias e, dado esta dificuldade, a descrição mais comum trata os vários estágios de evolução do sistema através de diferentes modelos para cada etapa do processo de colisão. Nestes modelos, o sistema passa pela fase de QGP simulada utilizando-se hidrodinâmica relativística e, após a fase de expansão e resfriamento, ele hadroniza através do sampleamento da hiper-superfície de energia e momento. Os hádrons resultantes então interagem tanto elástica como inelasticamente numa fase hadrônica simulada utilizando-se modelos de cascatas de hádrons, até que as densidades destes hádrons seja baixa o suficiente para que não hajam mais interações. Já que estes modelos utilizam várias hipóteses físicas e componentes para calcular os hádrons resultantes, eles são conhecidos como *modelos híbridos*.

Neste trabalho, propõe-se o estudo do fluxo elíptico v_2 de partículas carregadas criadas em colisões de Pb-Pb nas energias de $\sqrt{s_{\mathrm{NN}}} = 2.76$ TeV usando um modelo híbrido que emprega o simulador hidrodinâmico MUSIC assim como o UrQMD para emular a fase hadrônica. Este v_2 final será então comparado com condições iniciais assim como a dados experimentais da colaboração ALICE nestas mesmas energias.

Palavras-chave: colisões de íons pesados, fenomenologia, plasma de quarks e glúons.

List of Figures

Summary

List of Figures

Introduction

To contextualize the project and develop a necessary theoretical basis to the comprehension of the results that will be discussed in the next chapters, this introductory chapter is meant as a review of the main properties of the Standard Model of Particles, the main terminology of the area and the available experimental observables.

1.1 The Standard Model of particle physics

The area of high-energy particle physics is flourishing with areas of intense research and great relevance. Based in the Standard Model, of broad applicability and with a history of success through its experimental verifications, a current subject of interest is the investigation of evidences of the existence of a state of matter denominated Quark Gluon Plasma (QGP). Due to its high complexity, the description of nuclear collisions through a complete theoretical set of equations that includes Quantum Chromodynamics (QCD) is still an open challenge in high-energy physics, which prompts its study, with the objective of correlating its predictions with experimental data, to be done with phenomenology.

To understand the composition of known matter, it is first necessary to define the structure of the Standard Model, which is composed of elementary particles and the mediators of the three forces that are encased in the theory. The first table below lists those elementary particles in order of discovery, where Q stands for the electrical charge of said particle, and numbers I to III represent the generation they belong to; where the second connects bosonic mediators (spin 1 particles that obey Bose-Einstein statistics) of electromagnetic, electroweak and strong force to the previous particles.

Table 1.1: Elementary particles of the Standard Model

Leptons				Quarks			
Q	I	II	III	Q	I	II	III
-1	electron (e^-)	muon (μ^-)	tau (τ^-)	$-1/3$	down (d)	strange (s)	bottom (b)
0	electronic neutrino (ν_e)	muonic neutrino (ν_μ)	tauonic neutrino (ν_τ)	2/3	up (u)	charm (c)	top (t)

Its important to note that Table 1.1 does not enumerate the respective antiparticles (opposite charge Q) of each lepton and quark, for simplicity, and those particles can interact by the same means as the former ones. Also, excluding neutrinos, which decay as a consequence of an entirely different mechanism, the more massive quarks and leptons of generation III are able to decay into the lighter generation II particles, and those, in turn, can decay into the lightest generation I quarks.

Table 1.2: Physical forces of the Standard Model, its mediators and the respective Quantum Field Theory (QFT) that describes their interaction. The "Particle" section refers to particles that can interact through said mediators

	Photon (γ)	W^+, W^-, Z^0	g (8 gluons)
Interaction	Electromagnetic	Electroweak	Strong
Theory	Quantum Electrodynamics	Electroweak Theory	Quantum Chromodynamics
Charges	Electric	Electric and Weak	Color
Particles	Charged Leptons Hadrons and Quarks	Leptons, Hadrons and Quarks	Quarks and Gluons

Of the total 64 particles listed above, the ones that can be experimentally observed are leptons and hadrons (subdivided into baryons and mesons), the latter being composed by specific combinations of varying quarks without violating Pauli's Exclusion Principle of spin and a new quantum number known as "color", though not as a reference to electromagnetic radiation of those particles.

Each quark can have one of the three RGB (red, green and blue) colors, while gluons can carry two color charges (color and anticolor). With that in mind, baryons are modernly defined as particles encasing three RGB quarks, while mesons bear only two, with quarks of opposing color number. That definition follows the principle of null color, in which the combination of quarks must be such that the sum of color number in an observable particle is zero. This will be further discussed in the next section.

1.1.1 Quark confinement and Asymptotic Freedom

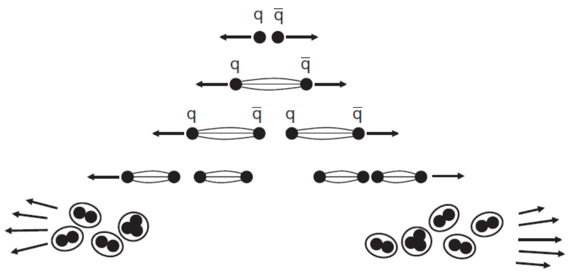

Figure 1.1: The hadronization process, in a qualitative description. Step three shows the formation of a new quark-antiquark pair when the energy stored in the color field is high enough for this process to occur. The final stage shows the resulting combination of quarks into hadrons. Adapted from [1].

A relevant property is that quarks can interact through gluons with each other and generate a resulting effective potential. It can be shown [1] that this potential assumes the following form for quark-antiquark states

$$V_{ef} = -\frac{4}{3}\frac{\alpha_s(r)\hbar c}{r} + kr \tag{1.1}$$

where $\alpha_s(r)$ indicates the intensity of the interaction of the quark duo, denoted as the strong force coupling constant. Notice that, for small distances r, V_{ef} has the same behavior of a Coulomb potential and, for larger distances, the same effective potential has an elastic dominion, which can be interpreted as a string tension between the quark pair, illustrated as the stretching seen above on Fig. 1.1.

In this first regime, lattice QCD calculations [6] also predicts an increase in the degrees of freedom of the system composed of quarks and gluons in extreme conditions of pressure and/or temperature, that is, a reduction of the effective potential perceived by those quarks, allowing an state of asymptotic freedom for those particles, which characterizes the quark-gluon plasma. This is also reflected in the values of the coupling constant at those regimes, of around $\alpha_s \approx 0.1$, a condition that allows perturbation theory to be applied to QCD and quarks can then be treated as quasi-free particles.

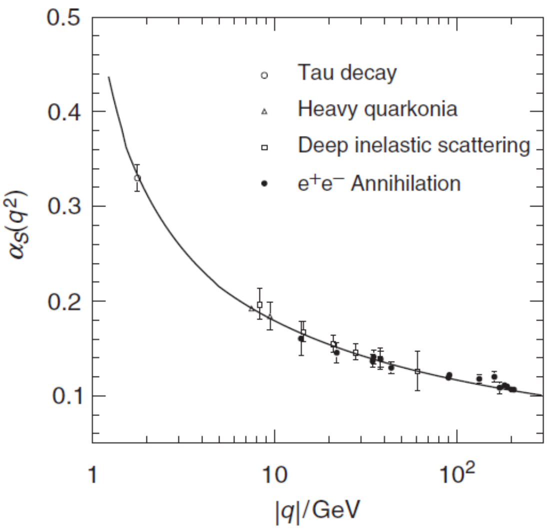

Figure 1.2: Different measurements of the coupling constant α_s for ranging ($|q|$), where the black curve indicates the theoretical prediction where perturbative lattice QCD calculations can be applied. Adapted from [1].

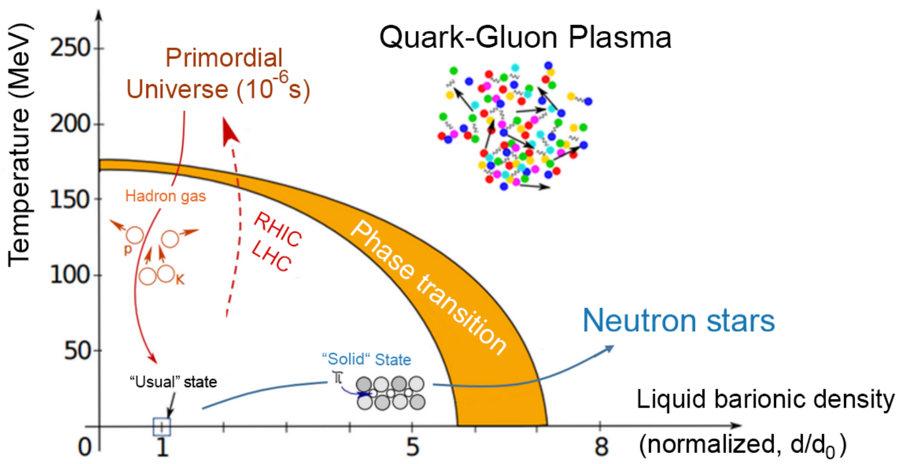

Figure 1.3: Schematic representation of the phase transition predicted by lattice QCD calculations in different regimes of temperature and barionic density. Adapted from [2].

For experiments involving collisions of particles, where the temperature can surpass the necessary 150 to 200 MeV [6] for the phase transition to QGP to occur, as shown above, it would be possible to observe evidence of the existence of this state of matter, and detect observables correlated to this event is one of the motivating objectives of the ALICE collaboration, at CERN, dedicated to the analysis of heavy-ions and being essential to provide the experimental basis data that was used throughout this work.

1.2 Collision stages and initial conditions

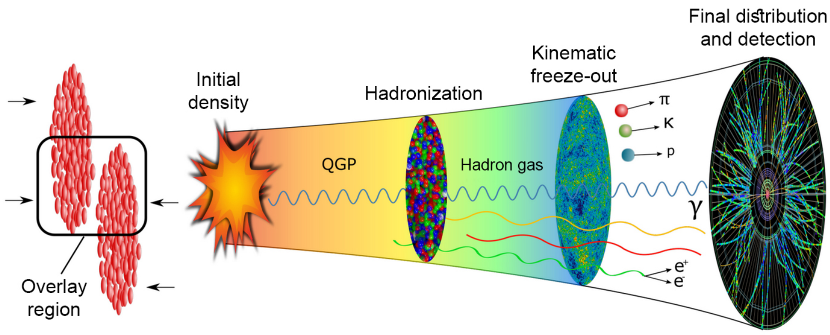

Figure 1.4: Representation of each heavy-ion collision stage.

To first understand and model the processes of heavy-ion collisions, the stages of scattering involved in such collisions are to be defined. As shown above, for ultrarrelativistic particle collisions, the phases are as follows:

1. **Hard interaction**, which comprises the first interactions between colliding ions;
2. **Thermalization**, with an intense production of particles and the expansion of the system. The proposal is that QGP would be formed in ths stage, for a time span of about 10^{-15} fm/c;
3. **Hadronisation**, that is, quarks combines into color singlets when temperature and density are sufficiently low;
4. **Chemical *Freeze-out***, marked by the end of inelastic interactions and the constancy of the chemical composition of the system;
5. **Kinematic *Freeze-out***, ceasing the interaction between hadrons. The expansion ends with a low energy density that characterizes this stage.

It's important to notice that experimental measurements can only be performed after the last stage described above, and the observables that can be acquired will be detailed in the next section. However, it's crucial to understand the initial conditions of the scattering process, where two geometrical variables are of great importance: impact parameter (b) and the collision's centrality (c).

The first (b) can be defined by the transversal distance separating the colliding centers, as shown in Fig. 1.4 on the overlay region. This variable will determine the influence that the distance of collision between nucleons will have on the observed result. As for the second (c), the impact parameter is used to define a region of superposition of the two centers or, in other words, forming a fraction of the cross section.

$$c = \frac{\int_0^b \frac{d\sigma}{db'} db'}{\int_0^\infty \frac{d\sigma}{db'} db'} \tag{1.2}$$

Lastly, it is necessary to model each stage of the collision, from the initial contact between the nucleons and the detection of experimental observables. For this task, phenomenological models have be employed, and those used throughout this project will be discussed in depth in chapter 2.

1.2.1 Kinematic variables

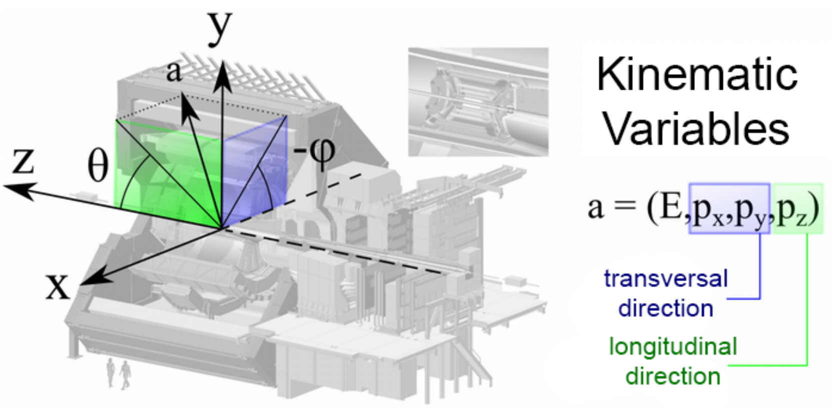

Figure 1.5: Representation of the collider and of the standard reference axis adopted throughout the methodology of this project.

To characterize experimentally the resulting particles of ultrarrelativistic collisions, two types of geometrical variables are employed: transversal and longitudinal, defined in the same way as shown in Fig. 1.5. The essential one for the longitudinal direction is denoted pseudo-rapidity, η, used as an alignment paramenter between the beam and the particle of interest's trajectory. η is defined as

$$\eta = \frac{1}{2} ln \left(\frac{|\mathbf{p}| + p_z}{|\mathbf{p}| - p_z} \right) = -ln \left(tan \left(\frac{\theta}{2} \right) \right) \tag{1.3}$$

As for the transversal direction, the most relevant and employed variable to characterizes scattering products is the transversal momentum, p_T, that is given as follows

$$p_T^2 = p_x^2 + p_y^2 \tag{1.4}$$

Another essential information that can be extracted from a set of events is the multiplicity of detected particles, which allows the experimental determination of the centrality of collision. The reason for applying this alternative procedure of measurement instead of measuring the impact parameter is that, on the scale of 10^{-15}m, b is inaccessible to experimentation, and can only be known through relations to other experimentally viable variables.

To extract the centralities intervals of a certain set of events quantitatively, it is first necessary to define a minimum bias, where all possible collisions of such a set are accounted for. The bias yield is then split into defined intervals, starting from the maximum value of multiplicity (N_{ch}) of the measurement, as shown below in Fig. 1.6 . Taking the interval of centrality of 0-5 % as an example, it would correspond to the first 5% higher values of N_{ch}, and, as another example, the overlap region of 0-40% and 0-50% would define the centrality class of 40-50%.

One can also use entropy, or energy densities, intervals as a way to determine the centrality classes of a set of events, defining entropy profiles in the same way as it is done with multiplicity intervals. Note that, greater collision energies will then impact on both observed and simulated energy densities, and consequently on how the centrality of a set of events will be determined.

The energy of collision with respect to the laboratory frame is then defined as follows. Considering a collision between two nucleons, A and B, where A is the projectile and B the target (at rest on the laboratory frame) the equation that defines the energy of collision in both the lab and center of mass frames comes from the relativistic energy relation

$$E_{cm} = \sqrt{(2E_{lab} + m_B c^2) m_B c^2 + m_A^2 c^4} \tag{1.5}$$

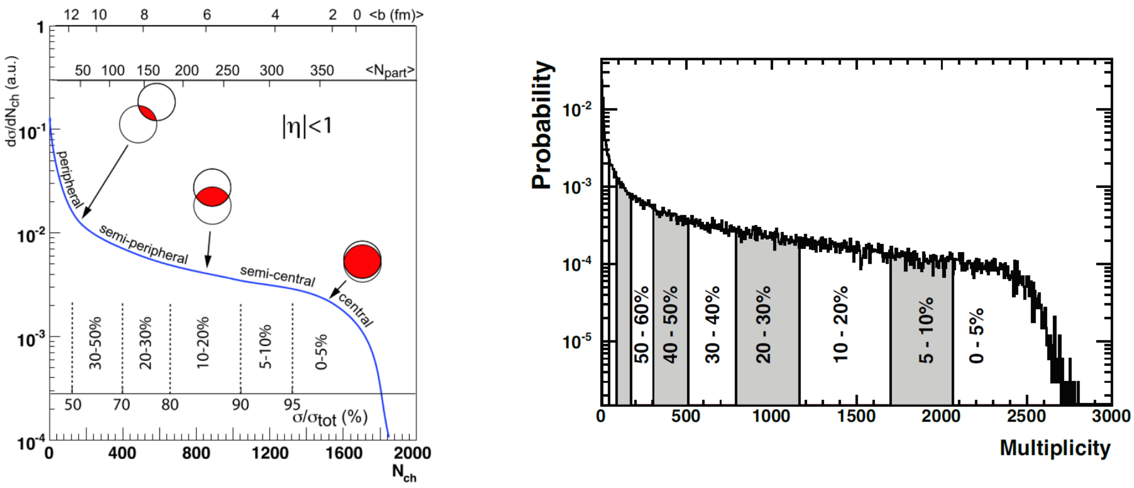

(a) (b)

Figure 1.6: (a) The relation of impact parameter and multiplicity to centrality intervals. Adapted from [3]; (b) Multiplicity distribution on a Pb-Pb collision at 2.76 TeV. Extracted from [4].

where E_{cm} is the energy in the center of mass frame, E_{lab} the energy on the lab frame, m_A and m_B the masses of nucleons A and B, respectively, and c the speed of light. In collider experiments, ions are collided while traveling in opposite directions and, considering the nucleons to be identical, the energy of collision is simply the sum of the energies of the beams, where this quantity is a Lorentz invariant and generally expressed as $\sqrt{s}$ [7].

1.3 Anisotropic flow and the method of cumulants

An interesting phenomenon observed in experimental measurements of heavy-ion collisions is a rather collective behavior of the produced particles, which can be verified by the anisotropic distribution of those particles, where the experimental observables are based on the angular correlation of the measured byproducts. This collective behavior allows for a hydrodynamic approach to such a system and, noting that the energy density and temperature criteria are chosen such that the quark-gluon plasma can exist, this method permits the study of this state of matter. In this section, the methodology used to study the correlation of said particles, as means to understand the anisotropy of a heavy-ion collision, will be defined.

Firstly, taking a Fourier series of the equation describing the azimuthal distribution of particles,

$$E\frac{d^3N}{d^3p} = \frac{1}{2\pi p_t}\frac{d^2N}{d\eta dp_t}\left(1 + \sum_{n=1}^{\infty} 2v_n cos(n[\phi - \Psi_{RP}])\right) \tag{1.6}$$

with E as the energy of the particle, one arrives at the differential coefficients v_n of the series, usually functions of transverse momentum and rapidity of the particles, which are given by

$$v_n \approx \langle cos(n[\phi - \Psi_{RP}])\rangle \tag{1.7}$$

where $\langle ... \rangle$ denotes the mean taken first onto the first subset of particles in each event and, after that, taken over all events; for the angular variables, ϕ denotes the azimuthal and Ψ_{RP} the reaction plane angle, defined as $\Psi_{RP} = 0$ in the initial condition generator. Also, n defines the nth coefficient of the series, where the first three coefficients, v_1, v_2, v_3, are designated as directed flow, elliptic flow and triangular flow, in this order. It's also important to note that the last two react to different types of asymmetry in the event plane. Shown below is a representation of the momentum anisotropy of the final distribution of particles to the elliptic flow. Note that the initial geometry of the collision is essentially elliptic.

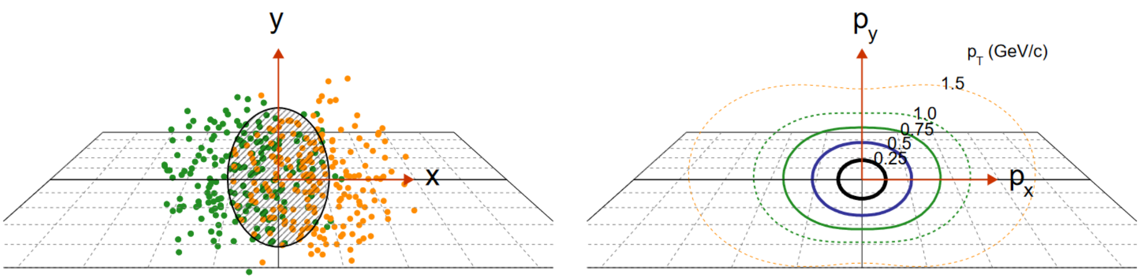

Figure 1.7: A schematic representation of a non-central collision, to the left, and the profile of the surface modeled by the v_2 coefficient, to the right, with each average radius representing the p_T of the particles and the anisotropy of the ring indicating the magnitude of the elliptic flow coefficient [5].

An important remark can be made on the impact of E into the anisotropy of the system. As the collision energy increases, so does the gradients observed in 1.7, and consequently the geometry of the system is altered by this parameter. With v_2 being an intrinsically geometric variable, the collision energy of the simulated events is essential for all performed analysis.

Having defined the flow coefficients, their calculation can be done through two approaches: using the event plane method, only available on simulation techniques and not employed on the determination of particle's correlation, or the cumulant method. This work will focus only on the study done through the latter.

The cumulant method can be defined as a technique that determines the correlation between produced particles by analysing the global anisotropy of the event, defined in the initial moments of the collision. The main hypothesis is that, if each particle is somehow correlated to this global anisotropy, then those will also have a angular correlation between themselves.

The development of such coefficients will be restricted to the second and fourth order correlations, with higher order results given in [8]. A relevant remark is that increasing orders of correlation on flow coefficients turns the results less sensitive to local correlations, resulting in $v_2\{2\}$ being the best choice to study a local phenomena, such as correlations from particle decays, and $v_2\{4\}$ more fit to observe the global aspect of particle emission.

The technique used to do such calculations is named direct cumulant, or Q-cumulant method. The implementation into the analysis macro is quite simple, and avoiding a potential issue with encased loops, as discussed below, can be also a efficient way of calculating cumulants. Starting from the definition of the Q-vector for an given harmonic of n-th order, Q_n, which will be used for correcting the loops issue in the computational approach,

$$Q_n = \sum_{i=1}^{M} e^{in\phi_i}, \quad \begin{cases} |Q_n|^2 = \sum_{i,j=1}^{M} e^{in(\phi_i-\phi_j)} = M + \sum_{i,j}' e^{in(\phi_i-\phi_j)} \\ |Q_n|^4 = Q_n Q_n Q_n^* Q_n^* = \sum_{i,j,k,l=1}^{M} e^{in(\phi_i+\phi_j-\phi_k-\phi_l)} \end{cases} \tag{1.8}$$

where M is the multiplicity, ϕ the angles and the sum $\sum'$ must be done for different indices. The mean of the correlations for two and four particles, for each event, can then be defined respectively as

$$\langle 2 \rangle = \langle e^{in(\phi_1-\phi_2)} \rangle = \frac{1}{P_{M,2}} \sum_{i,j}' e^{in(\phi_i-\phi_j)} = \frac{|Q_n|^2 - M}{M(M-1)} \tag{1.9}$$

$$\langle 4\rangle = \langle e^{in(\phi_1+\phi_2-\phi_3-\phi_4)}\rangle = \frac{1}{P_{M,4}}\sum_{i,j,k,l}{}' e^{in(\phi_i+\phi_j-\phi_k-\phi_l)} = \\ = \frac{|Q_n|^4+|Q_{2n}|^2-2\Re|Q_{2n}Q_n^*Q_n^*|}{M(M-1)(M-2)(M-3)} - 2\frac{2(M-2).|Q_{2n}|^2M(M-3)}{M(M-1)(M-2)(M-3)} \tag{1.10}$$

where $P_{n,m} = n!/(n-m)!$.

Now, taking the mean over the events, one arrives at

$$\langle\langle 2\rangle\rangle = \langle\langle e^{in(\phi_1-\phi_2)}\rangle\rangle = \frac{\sum_{events}(W_{\langle 2\rangle})_i\langle 2\rangle_i}{\sum_{events}(W_{\langle 2\rangle})_i} \tag{1.11}$$

$$\langle\langle 4\rangle\rangle = \langle\langle e^{in(\phi_1+\phi_2-\phi_3-\phi_4)}\rangle\rangle = \frac{\sum_{events}(W_{\langle 4\rangle})_i\langle 4\rangle_i}{\sum_{events}(W_{\langle 4\rangle})_i} \tag{1.12}$$

with $W_{\langle 2\rangle}$ and $W_{\langle 4\rangle}$ are used to minimize the effects of the multiplicity fluctuation in each event, and given by

$$W_{\langle 2\rangle} = M(M-1) \tag{1.13}$$

$$W_{\langle 4\rangle} = M(M-1)(M-2)(M-3) \tag{1.14}$$

notice that Eqs. 1.13 and 1.14 appear, respectively, on the denominators of Eq. 1.9 and 1.10.

Now, with those definitions, it is possible to define the cumulant coefficients for the events, and arrive then at the flux coefficients

$$\boxed{c_n\{2\} = \langle\langle 2\rangle\rangle \Rightarrow v_n\{2\} = \sqrt{c_n\{2\}}} \tag{1.15}$$

$$\boxed{c_n\{4\} = \langle\langle 4\rangle\rangle - 2.\langle\langle 2\rangle\rangle^2 \Rightarrow v_n\{4\} = \sqrt[4]{-c_n\{4\}}} \tag{1.16}$$

Finally, it is necessary to define de differential flow coefficients for two and four particle correlation. Their final form is given by the following relations

$$\boxed{d_n\{2\} = \langle\langle 2'\rangle\rangle \Rightarrow v_n'\{2\} = \frac{d_n\{2\}}{\sqrt{c_n\{2\}}}} \tag{1.17}$$

$$\boxed{\langle\langle 4'\rangle\rangle - 2.\langle\langle 2'\rangle\rangle^2 \Rightarrow v_n'\{4\} = \frac{d_n\{4\}}{(-c_n\{4\})^{3/4}}} \tag{1.18}$$

where $d_n\{2\}$ and $d_n\{4\}$ are, respectively, the coefficients of second and fourth order for particle detectors with uniform azimuthal acceptance, being this the case for the simulated events in this project. To arrive at Eqs. 1.17 and 1.18, firstly it is necessary to define the quantities vector-p and vector-q

$$\begin{cases} p_n = \sum_{i=i}^{m_p} e^{in\psi_i} \\ q_n = \sum_{i=i}^{m_q} e^{in\psi_i} \end{cases} \tag{1.19}$$

where p_n encases particles with some characteristic (or characteristics) of interest, such as intervals of p_T or rapidity, denoted as *Particle of Interest* (POI), and q_n refers to particles used in the calculations of the reference flux, known as *Reference Flow Particle* (RFP). This coefficient also subtracts effects of self correlation.

With that done, $\langle\langle 2'\rangle\rangle$ and $\langle\langle 4'\rangle\rangle$ will then be calculated by taking the same two means as before (by event and for all events) and rewritten using the Q-vector, q-vector and p-vector formalism

$$\langle 2'\rangle = \langle e^{in(\phi_1-\phi_2)}\rangle = \frac{1}{m_pM-m_q}\sum_{i=1}^{m_p}\sum_{j^*=1}^{M} e^{in(\phi_i-\phi_j)} = \frac{p_nQ_{n^*}-m_q}{m_pM-m_q} \tag{1.20}$$

$$\begin{aligned}\langle 4'\rangle = \langle e^{in(\phi_1+\phi_2-\phi_3-\phi_4)}\rangle = \frac{1}{(m_pM-3m_q)(M-1)(M-2)}\sum_{i=1}^{m_p}\sum_{j^*,k^*,l^*=1}^{M} e^{in(\phi_i+\phi_j-\phi_k-\phi_l)} = \\ = (p_nQ_nQ_n^*Q_n^* - q_{2n}Q_n^*Q_n^* - p_nQ_nQ_{2n}^* - 2Mp_nQ_n^* - 2m_q|Q_n|^2 + 7q_nQ_n^* - Q_nq_n^* \\ q_{2n}Q_{2n}^* + 2p_nQ_n^* + 2m_qM - 6m_q)/[(m_pM-3m_q)(M-1)(M-2)]\end{aligned} \tag{1.21}$$

Using then

$$w_{\langle 2'\rangle} = m_pM - m_q \tag{1.22}$$

$$w_{\langle 4'\rangle} = (m_pM-3m_q)(M-1)(M-2) \tag{1.23}$$

to as weights for the following relations, one arrives at

$$\langle\langle 2' \rangle\rangle = \langle\langle e^{in(\phi_1 - \phi_2)} \rangle\rangle = \frac{\sum_{events} (W_{\langle 2' \rangle})_i \langle 2' \rangle_i}{\sum_{events} (W_{\langle 2' \rangle})_i} \tag{1.24}$$

$$\langle\langle 4' \rangle\rangle = \langle\langle e^{in(\phi_1 + \phi_2 - \phi_3 - \phi_4)} \rangle\rangle = \frac{\sum_{events} (W_{\langle 4' \rangle})_i \langle 4' \rangle_i}{\sum_{events} (W_{\langle 4' \rangle})_i} \tag{1.25}$$

which results in Eqs. 1.17 and 1.18. For the initial proposal of the method and a greater level of detail on its development, see [9].

The phenomenological model

In this section, the adopted methodology of simulation of events will be described, presenting the employed packages in each stage of the collision, as show below in Fig. 2.1. After that, samples generated through this technique for different collision energies will be shown and compared to experimental data of the ALICE collaboration.

2.1 Simulation chain

As presented in the previous section, heavy-ion ultrarrelativistic collisions consists on basically six main stages, from where results the experimental observables of interest to a comparison with QCD based simulations. The code packages used in each of these steps are shown above.

2.1.1 Initial condition generators and pre-equilibrium dynamics

TRENTo: Responsible for the generation of a set of initial conditions that will be used in the hydrodynamics stage. The model is supported by an Monte Carlo algorithm to generate the initial entropy profiles, describing the multiplicity distributions of nucleon-nucleon collision of interest and staying consistent with experimental bounds. Its defining characteristic is to present those results without assuming entropy production, thermalization or pre-equilibrium dynamics mechanisms. A throughout description of both the

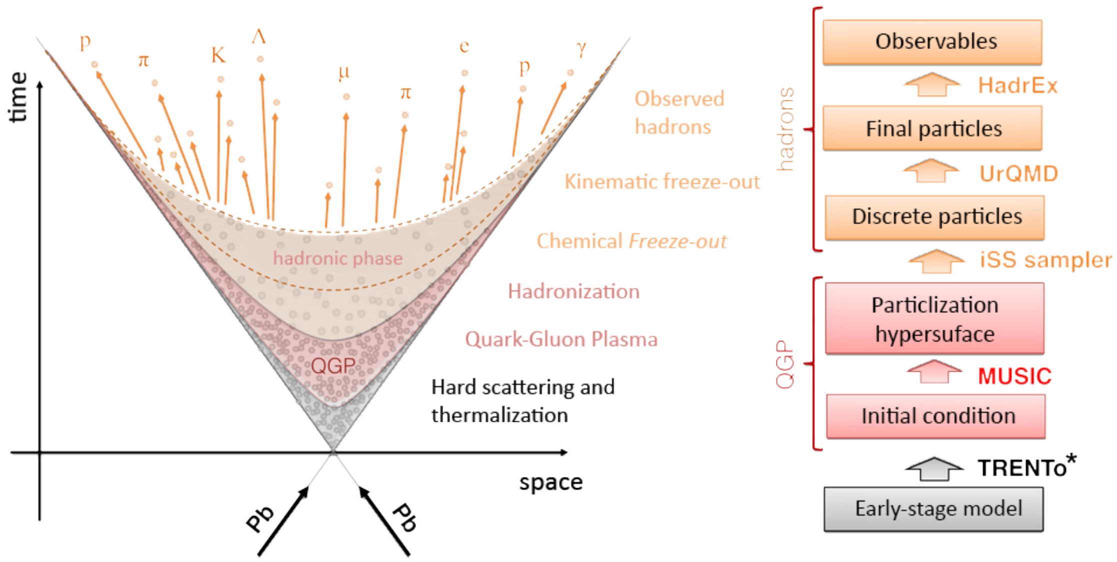

Figure 2.1: Stages of a heavy-ion collision, here showing the Pb-Pb process and the possible hadron byproducts in the final step. In the right corner, the used packages for event generation.

theory used and its formulation into the code can be found in [10, 11].

Kompost: Applies pre-equilibrium dynamics, which can be summarized as a small evolution of the equation of state (EoS) of the system, to TRENTo's generated initial conditions [12]. The evolution ceases when the system is sufficiently close to thermal equilibrium, a prerequisite that allows viscous hydrodynamics to be employed in the posterior analysis.

2.1.2 Hydrodynamic evolution in MUSIC and particlization

In the QGP thermalization stage, the MUSIC package has the task of describing the relativistic hydrodynamics evolution of the previously given initial conditions. To understand the methodology employed, it is first necessary to note that, in the relativistic hydrodynamics approach, the main hypothesis for a fluid-like behavior is that the net energy and number of particles is conserved. Those conditions can be expressed by the following set of equations

$$\partial_\mu N^\mu \quad , \quad \partial_\mu T^{\mu\nu} = 0 \tag{2.1}$$

where $T^{\mu\nu}$ is the symmetric energy-momentum tensor that will describe the space-time evolution of the system, and N^{μ} the 4-current of the plasma. The former can be decomposed in four fields, namely energy density (ϵ), flow velocity (u^{μ}), the shear stress tensor ($\pi^{\mu\nu}$), and the bulk pressure (Π), which are parameters that enter the numerical calculations of the MUSIC package. The difference between viscous and non-viscous (or ideal) hydrodynamics lies in the parameters $\pi^{\mu\nu}$ and Π, in which both are taken to be zero in ideal hydrodynamics.

With the appropriate equations of state (EoS), MUSIC can then numerically solve Eq. 2.1 using hyperbolic coordinates and save the resulting fluid for latter stages. The chosen equations for a viscous hydrodynamics evolution of the system can be found on [13, 14], meant for strongly-coupled quark-gluon plasma. Other types of EoS capable of describing the s-QGP are currently under study by the research group.

For an in-depth description of the package's implementation of the previously described theory, see [15].

2.1.3 Freeze-out stages and observables

It must be noted that the hydrodynamics stage needs to end with a well defined criteria, because this will define the conversion of the evolved fluid into hadrons. This stage is named *particlization* and is assumed to happen at a given temperature (or energy density, through the EoS), in the range of 150 MeV $<$ T $<$ 200 MeV. The evolution is considered complete if all points in the system are below the said criteria. For a more realistic approach, the freeze-out temperature, from which the decoupling detailed previously may occur, is split into two different stages: the chemical phase (with T_{ch}), in which the inelastic scattering of hadrons ceases, creating a constant density of species of particles, and the kinetic phase (T_{kin}), ending the elastic scattering of those hadrons. These two criteria are applied into the solution of Cooper-Frye's equation.

The next step is the conversion of the previous hydrodynamic results into particles, in which the Cooper-Frye formula, as shown below, and its associated procedure [16] is used to model this phase. The main characteristic of this stage is the free propagation of particles, decoupled from the previous collective behavior of the system as a consequence of its expansion.

$$E\frac{d^3N_s}{dp^3} = g_s \int_\Sigma d\Sigma_\mu P^\mu f_s(P, \epsilon, u^\mu, \pi^{\mu\nu}, \Pi) \quad (2.2)$$

In the Cooper-Frye formalism, the momentum distribution of the species of hadrons inside the fluid is integrated through the particlization hypersurface (of section $d\Sigma_\mu$) of this same fluid, and the result of the numerical solution of this equation is the distribution of momentum Ed^3N_s/dp^3 of each hadron.

iSS sampler: To end the hydrodynamics stage and act as a complement to MUSIC, the sampler simulates the hadron formation on the system with the usage of a Monte Carlo algorithm to solve Eq. 2.2. These particle distributions will then be stored to the last stage of the chain. The code can be found on [17];

UrQMD: In this final stage, it is necessary to simulate decays of hadrons, allowing the previous results to be transformed into a set of particles that can then be compared to experimental observations. This package then describes the dynamics of the observables byproducts of the collision chain, using a transport model and the outputs given in the earlier stages of the simulation. The documentation can be found on [18];

HadrEx: The last set of codes for the simulation chain is the package that does the conversion of the output given by UrQMD to a more convenient format for data analysis programs such as ROOT. It was specially developed by the research group for this specific task.

2.2 Method of event analysis

With the completion of the event chain for a given Pb-Pb collision energy and with the generated events available, the next step consists of writing codes capable of extracting results of interest from those events. The following sections and chapter 3 details the method employed on the creation of those codes.

As a note, all uncertainties from simulated data were propagated according to the method described on [19], with all figures of chapter 3 including error bars.

2.2.1 The ROOT package of data analysis

Being the central piece of this project, the toolbox provided by the program ROOT allows the efficient processing of the generated data by the chain, using the programing language C++. All of the graphics to be presented where done employing this tool and its library basis *.

*Version 6.16/00 - 2019-01-23

Results

In this section, the analysis done for elliptical flow will be presented and discussed in depth, such as the distribution of $v_2\{2\}$ and $v_2\{4\}$ within p_T and centrality intervals, using the angular distribution of particles as a function of the scattering angle ϕ as a baseline model. The main objective of this development is to compare simulations with and without the Kompost pre-equilibrium model to experimental data from the ALICE collaboration.

On all studies presented in this chapter, all data is integrated on η. The interval of pseudorapidity used to do this was $|\eta| < 0.8$.

Also, an important remark is that it is possible to simulate any centrality interval, here ranging from 0-5% (central events) to 70-80% (peripheral events), using the initial entropy densities of the events. However, the focus of this work was directed at those intervals that are directly comparable with experimental data. In section 3.1 and section 3.3, the centrality interval of 40-50% was given special attention, since experimental measurements in that event class are readily available and elliptic flow is a more prominent phenomenon [20].

3.1 Angular distribution of particles

In order to determine if the azimuthal anisotropy of particle emission is correlated with the simulated event plane, the angular distribution of particles with respect to this plane were calculated, and this result also enabled the creation of a baseline for comparison with v_2 coefficients via cumulants. A specific code was written to run such analysis into the generated events of both chains, namely one using TRENTo only initial conditions and the second employing pre-equilibrium dynamics applied to those conditions. This code also extracts the flow dependence with transverse momentum, integrated and differential flow for each centrality interval of the analyzed events, to be presented in the next sections. Other variables used through this analysis are: rapidity and pseudo-rapidity distribution and multiplicity of events.

It is important to note that such analysis of angular distribution is only accessible through simulation techniques, as the event plane is not a measurable quantity, thus giving the baseline aspect mentioned before. For both figures below, the interval of transverse momentum is $0 < p_T < 4.5$ GeV/c.

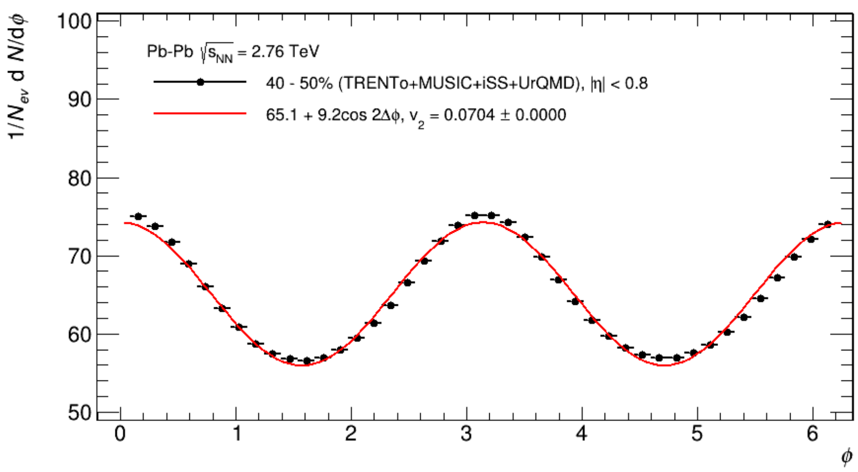

Figure 3.1: Angular distribution of particles for peripheral events using initial conditions given by TRENTo only, normalized by the number of events.

Two results are of note from these two figures. Firstly, there is a clearly oscillation pattern on the data that can be described by a function of the form $\cos[2(\phi - \Psi)]$ and appearing as a result of the elliptical form of the initial geometry. This shows the elliptic

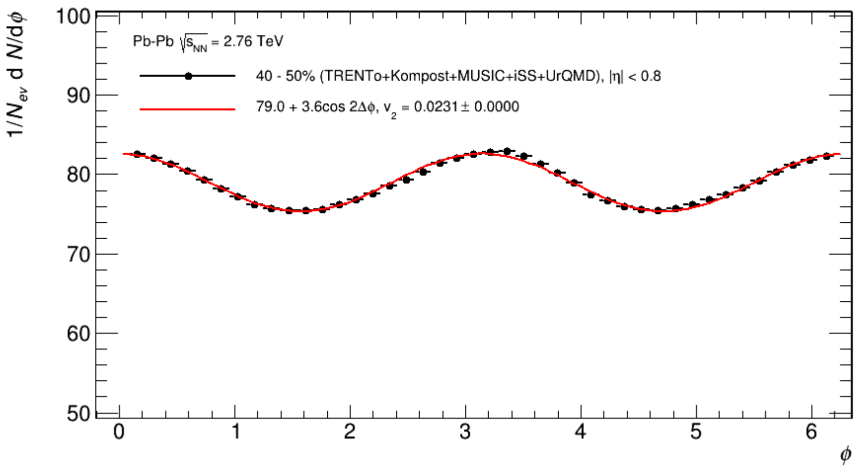

Figure 3.2: Angular distribution of particles for peripheral events, for the TRENTo+Kompost combination, normalized by the number of events.

flow on both data sets, and its value is given by the Fourier expansion Eq. 1.6 and its coefficient on Eq. 1.7. The red curves are fits of this equation to the distribution data.

Secondly, on the pre-equilibrium dynamics model, of Fig. 3.2, the oscillation of data is smaller than the one observed in Fig. 3.1. Also, the values of densities are slightly bigger on the latter figure. The reason for this behavior is the strong dependence of such results with the p_T distribution of particles: the Kompost package, when applying pre-equilibrium dynamics, significantly alters the transverse momenta of such particles, and this is reflected on the smaller oscillation of the angular histogram.

3.2 Elliptic flow as a function of centrality

The next analysis consisted in using the available v_2 histograms for each centrality interval, integrated in the transverse momenta range of $0.2 < p_T < 5$ GeV/c - the same of the experimental results used. As the elliptic asymmetry of the initial geometry changes with the centrality of the collision [21], it is expected that the following histograms must also show a centrality dependence.

With the results of the integrated flow for two and four particle correlation calculated, one can then create the curves shown in the figures below. Fig. 3.3 is a comparison of the two different particle correlation techniques, while Figs. 3.4 and 3.5 use experimental results that are shown in gray to contextualize the chain's outputs.

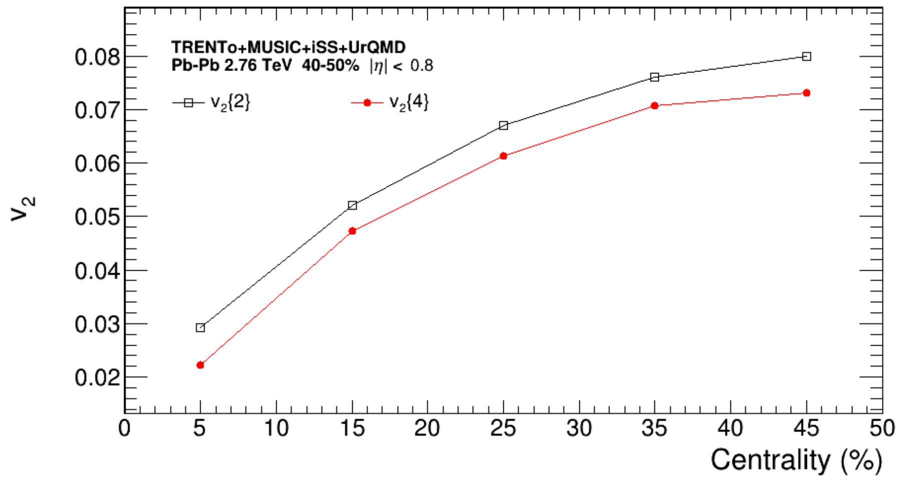

Figure 3.3: Comparison between the two and four particle correlation coefficients given by the TRENTo only approach to initial conditions.

Comparing firstly the flow outputs of initial conditions given only with the TRENTo package, it can be seen that the $v_2\{2\}$ outputs are higher than the four-particle flux coefficients $v_2\{4\}$ counterpart. This is also verified on experimental results, as shown comparatively below.

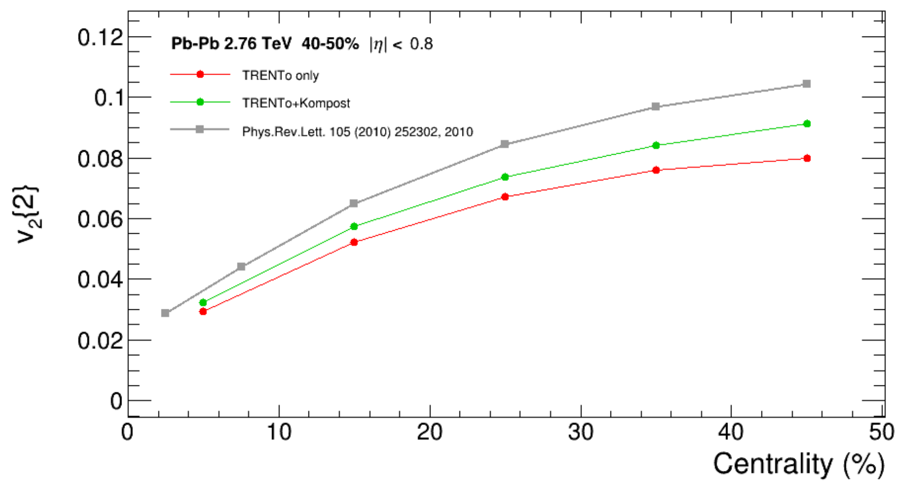

Figure 3.4: Dependency of the two-particle correlation elliptic flow, $v_2\{2\}$, to the centrality of each collision, for both pre-hydrodynamics approaches to initial conditions.

Notice that, for both approaches, the global values of v_2 are slighter lower than those from experimental results. Also, the pre-equilibrium approach not only follows the behavior of data but also points to a closer fit in both $v_2\{2\}$ and $v_2\{4\}$.

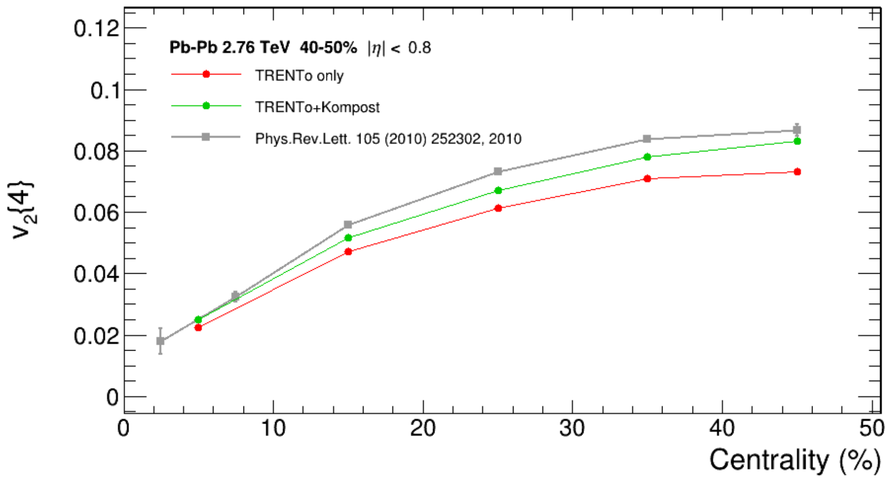

Figure 3.5: Dependency of the four-particle correlation elliptic flow, $v_2\{4\}$, to the centrality of each collision, for both pre-hydrodynamics approaches to initial conditions.

525 3.3 Flow as a function of transverse momentum

526 The objective of this section is to analyze the dependence of elliptic flow to transverse momenta of particles. To do so, first it is important to understand the way particles are distributed in a certain interval of momentum. Shown below are the densities of particles for both TRENTo only and TRENTo+Kompost chain's outputs for the centrality interval of 40-50%.

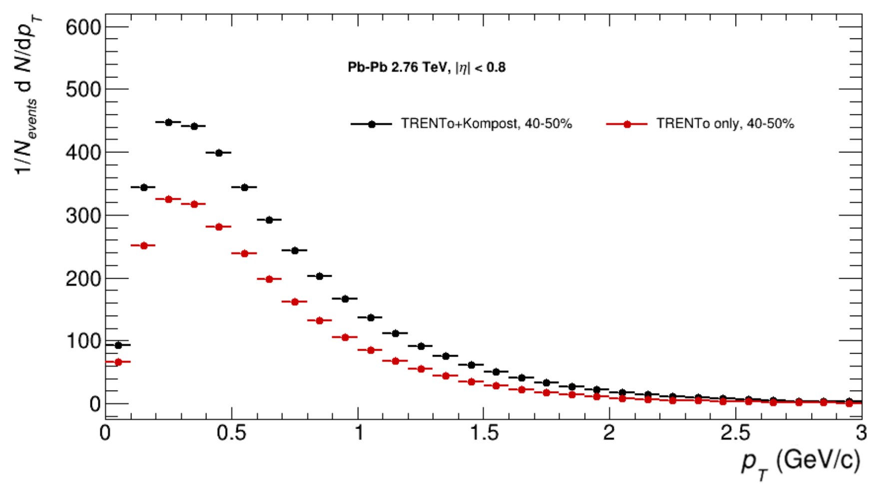

Figure 3.6: Particle densities for results of both simulation approaches, at $0 < p_T < 3$ GeV/c.

531 From those distributions, one can extract the mean transverse momentum, resulting

in

$$\langle p_T \rangle_{Kompost} = 0.67249 \pm 0.00007 \tag{3.1}$$

$$\langle p_T \rangle_{TRENTo} = 0.62368 \pm 0.00007 \tag{3.2}$$

As discussed on section 3.1, elliptic flow has a great dependence with transverse momentum, with results varying considerably depending on the p_T spectra of the sample. Eqs. 3.1 and 3.2 illustrates the mean p_T for the centrality interval used in the next figures, and the differences on elliptic flow shown in Figs. 3.4 and 3.5 also relies on those contrasting values for each centrality class, given that the flow coefficients are related to differential v_2 through an average weighted by the p_T distribution. This translates into larger values of p_T-integrated v_2 coefficients for higher values of $\langle p_T \rangle$.

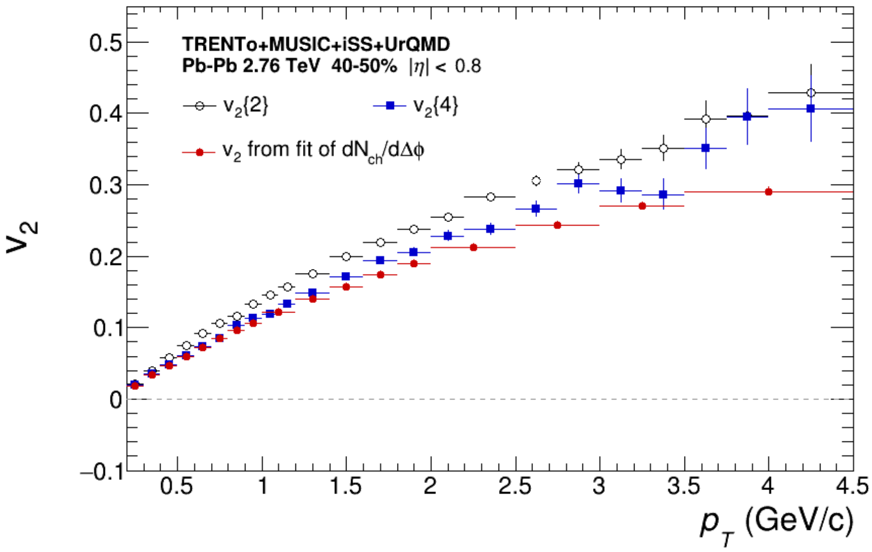

Figure 3.7: Differential elliptic flow for two and four-particle correlation for the transverse momentum interval of $0 < p_T < 4.5$ GeV/c.

Firstly, $v_2\{2\}$ and $v_2\{4\}$ are shown comparatively to the flow coefficient given from the fit of an angular distribution analogous to the ones presented in section 3.1. The difference is that now the fits are taken on distributions that are not integrated in a p_T interval. On a modification included into the analysis macro, a two-dimensional histogram is filled with the distribution of particles as a function of both p_T and ϕ, with Eq. 1.7 applied to this data as the fitting points shown in red. It can be seen in Fig. 3.7 that there is a considerable fluctuation of $v_2\{4\}$ above $p_T = 3.0$ GeV/c, and both it and $v_2\{2\}$

have increasing values when compared to the v_2 fit for this same set of data. Also, the behavior of four-particle correlation elliptic flow coefficients, $v_2\{4\}$, is less sensitive to local correlations, as discussed in section 1.3, which implies in values that are closer to the global behavior of the fit via angular distributions. The next two figures will then focus on comparing this coefficient for both initial condition approaches.

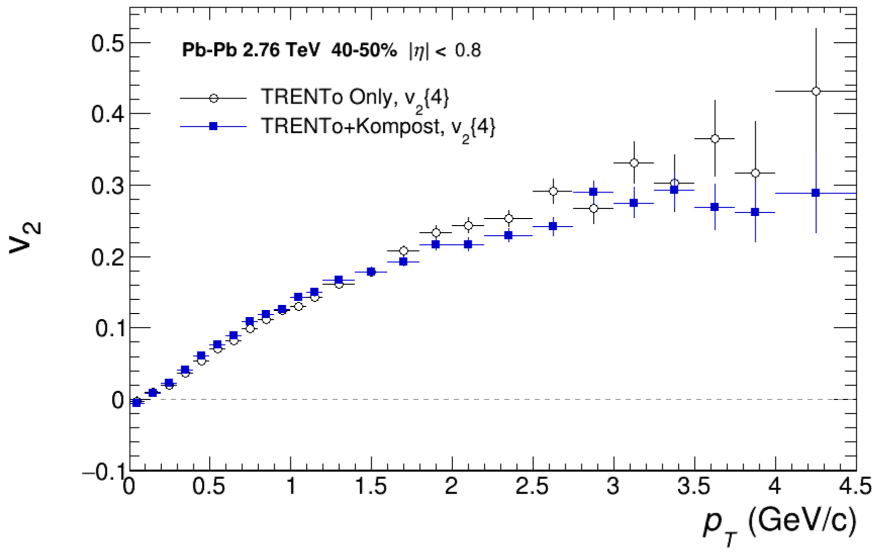

Figure 3.8: Differential elliptic flow from two-particle correlation for the transverse momentum interval of $0 < p_T < 4.5$ GeV/c, comparing the two simulation approaches and available experimental data.

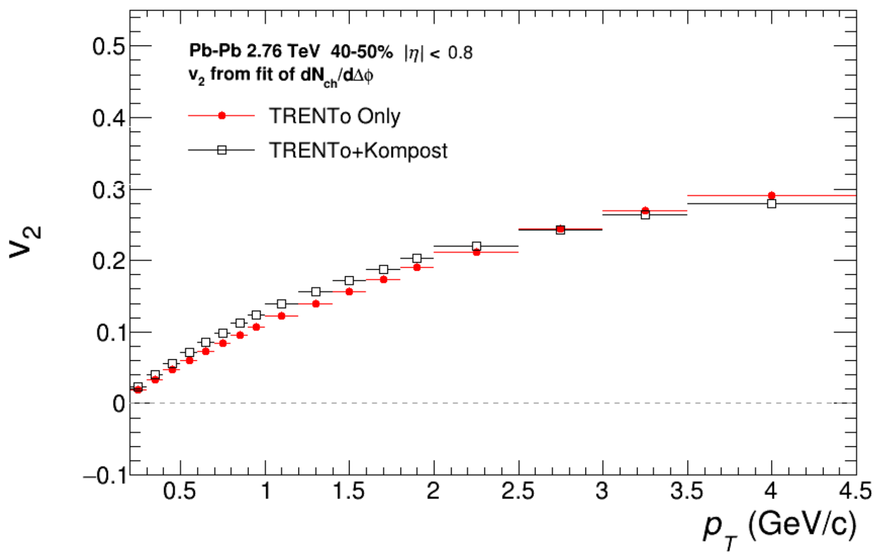

Figure 3.9: Elliptic flow coefficients as function of transverse momentum for both approaches to the initial conditions.

As in Fig. 3.7, the fluctuation at $p_T = 3.0$ GeV/c at Fig. 3.8 can also be observed for the pre-equilibrium chain outputs. However, the values and uncertainties of data for this interval are considerably lower. Then, when comparing the v_2 fits, in Fig. 3.9, it is evident that the TRENTo-Kompost outputs results in slighter higher values of fitted v_2 coefficients for the interval of transverse momentum $0.2 < p_T < 3.0$ GeV/c, decreasing after this value. This result corroborates to four-particle correlation having a significant influence into v_2 fit values.

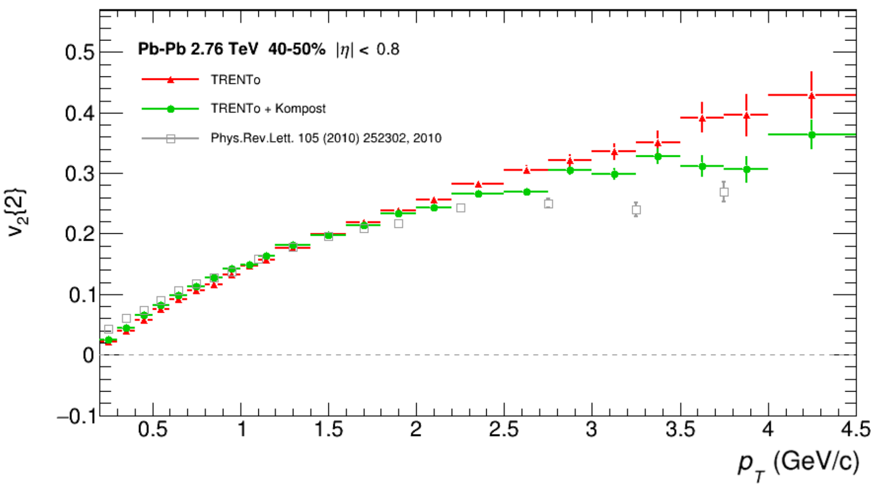

Figure 3.10: Differential elliptic flow from four-particle correlation for the transverse momentum interval of $0 < p_T < 4.5$ GeV/c, comparing the two simulation approaches and available experimental data.

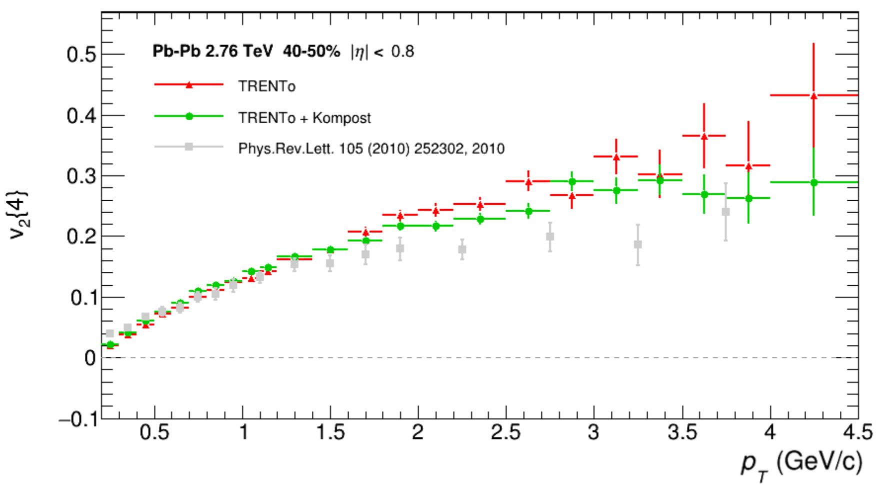

Figure 3.11: Differential elliptic flow from four-particle correlation for the transverse momentum interval of $0 < p_T < 4.5$ GeV/c, comparing the two simulation approaches and available experimental data.

Now, comparing both $v_2\{2\}$ and $v_2\{4\}$ from the two approaches to experimental data, the considerably lower increase in elliptic flow for pre-equilibrium chain's outputs on the interval of $p_T > 3$ GeV/c, evidenced before, than on those without this modification approaches the ALICE data more closely, pointing to pre-equilibrium dynamics being a more realistic approach to the QGP system.

Conclusions

In this work, a systematic study of the initial conditions and the anisotropy of a ultra-relativistic heavy-ion collision was done through a computational approach, using two different methods to simulate initial conditions and dedicating several packages to produce byproducts comparable to experimental observables.

Initially, the angular distributions for a Pb-Pb chain at 2.76 TeV were used as baseline for the following analysis, and illustrated the elliptical geometry of the initial conditions. The differences between the TRENTo only and the TRENTo+Kompost approaches already began to show on this baseline analysis, and were made evident through the next sections.

On section 3.2, integrated elliptic flow calculated from both methods was presented as a function of centrality and compared to experimental data, pointing to the influence of $\langle p_T \rangle$ into this variable. Then, on section 3.3, the mean p_T calculated for the centrality interval of 40-50% demonstrated this dependence of elliptic flow with transverse momentum intervals. Finally, for the differential flow presented on section 3.3, Figs. 3.7, 3.8, 3.9 and 3.11 showed $v_2\{4\}$ to be less sensitive to local correlations, such as decays, matching the anisotropy of particle emission versus the simulated event plane, which is consistent with its interpretation as being due to the collision geometry, and so resulting in an optimal choice to describe this anisotropy.

However, this approach has some constraints. It must be noted that, with increasing transverse momenta, not only fluctuations are more noticeable on differential elliptic flow, but uncertainties associated with high-momenta particles become relevant. Also, describing the quark-gluon plasma using an hydrodynamic approach is only useful up to a certain range of transverse momenta: for higher p_T, effects from perturbative QCD must be accounted for into the dynamics of the system. And even considering such effects, the computational time required to sample particles would become prohibitive for practical applications, if the entire phase space was analyzed.

Finally, the presented model still needs to be evaluated at a different collision energy, to verify quantitatively how this parameter will impact on the profiles used to select the centrality of an event and on the anisotropy of the system, as discussed in section 1.3. With recent data [22] from the ALICE collaboration at $\sqrt{s_{NN}} = 5.02$ TeV and the simulation chain's output for both initial conditions already available for the research group, studying the anisotropy of this system could be an extension of this work.

References

[1] Mark Thomson. *Modern Particle Physics.* Cambridge University Press, 2013.

[2] David Dobrigkeit Chinellato. *Estudo de estranheza em colisões próton-próton no LHC.* Doutorado em física, Universidade Estadual de Campinas, Instituto de Física Gleb Wataghin, Campinas, SP, 2012. http://repositorio.unicamp.br/jspui/handle/REPOSIP/278157.

[3] A. K. Chaudhuri. *A Short Course on Relativistic Heavy Ion Collisions.* IOP Publishing, 2014.

[4] K. et al Aamodt. Elliptic flow of charged particles in pb-pb collisions at $\sqrt{s_{NN}} = 2.76$ TeV. *Phys. Rev. Lett.*, 105:252302, Dec 2010.

[5] Paul Sorensen. Elliptic Flow: A Study of Space-Momentum Correlations In Relativistic Nuclear Collisions. In Rudolph C. Hwa and Xin-Nian Wang, editors, *Quark-gluon plasma 4*, pages 323–374. 2010.

[6] STAR Collaboration: J. Adams et al. Experimental and theoretical challenges in the search for the quark gluon plasma: The STAR Collaboration's critical assessment of the evidence from RHIC collisions. *Nucl. Phys.*, A757:102–183, 2005.

[7] C. Wong. *Introduction to high-energy heavy-ion collisions.* World scientific, Singapore, 1994.

[8] Jean-Yves Ollitrault, Arthur M. Poskanzer, and Sergei A. Voloshin. Effect of flow fluctuations and nonflow on elliptic flow methods. *Phys. Rev. C*, 80:014904, Jul 2009.

[9] Nicolas Borghini, Phuong Mai Dinh, and Jean-Yves Ollitrault. Flow analysis from multiparticle azimuthal correlations. *Phys. Rev. C*, 64:054901, Sep 2001. https://link.aps.org/doi/10.1103/PhysRevC.64.054901.

[10] J. Scott Moreland, Jonah E. Bernhard, and Steffen A. Bass. Alternative ansatz to wounded nucleon and binary collision scaling in high-energy nuclear collisions. *Phys. Rev. C*, 92:011901, Jul 2015. https://link.aps.org/doi/10.1103/PhysRevC.92.011901.

[11] Steffen A. Bass. Jonah E. Bernhard, J. Scott Moreland. Reduced thickness event-by-event nuclear topology (trento) official website. http://qcd.phy.duke.edu/trento/.

[12] Aleksi Kurkela, Aleksas Mazeliauskas, Jean-François Paquet, Sören Schlichting, and Derek Teaney. Effective kinetic description of event-by-event pre-equilibrium dynamics in high-energy heavy-ion collisions. *Phys. Rev.*, C99(3):034910, 2019.

[13] G. S. Denicol, H. Niemi, E. Molnar, and D. H. Rischke. Derivation of transient relativistic fluid dynamics from the Boltzmann equation. *Phys. Rev.*, D85:114047, 2012. [Erratum: Phys. Rev.D91,no.3,039902(2015)].

[14] E. Molnár, H. Niemi, G. S. Denicol, and D. H. Rischke. Relative importance of second-order terms in relativistic dissipative fluid dynamics. *Phys. Rev.*, D89(7):074010, 2014.

[15] Jean-François Paquet. *Simulating heavy ion collisions with MUSIC*, 2018. https://webhome.phy.duke.edu/~jp401/music_manual/.

[16] Fred Cooper and Graham Frye. Single-particle distribution in the hydrodynamic and statistical thermodynamic models of multiparticle production. *Phys. Rev. D*, 10:186–189, Jul 1974.

[17] Chun Shen. iss, monte carlo sampler for particle distribution from cooper-frye freeze-out procedure. https://github.com/chunshen1987/iSS.

[18] Frankfurt Institute for Advanced Studies. *Ultrarelativistic Quantum Molecular Dynamics (UrQMD) official website*. https://urqmd.org/.

[19] Harvard Instructional Physics Lab. A summary of error propagatione. http://ipl.physics.harvard.edu/wp-uploads/2013/03/PS3_Error_Propagation_sp13.pdf.

[20] K. et. al. Aamodt. Elliptic flow of charged particles in pb-pb collisions at $\sqrt{s_{NN}} = 2.76$ TeV. *Phys. Rev. Lett.*, 105:252302, Dec 2010. https://link.aps.org/doi/10.1103/PhysRevLett.105.252302.

[21] Rafael Derradi de. SOUZA. *Estudo dos efeitos de flutuações da condição inicial em colisões nucleares relativísticas.* Doutorado em física, Universidade Estadual de Campinas, Instituto de Física Gleb Wataghin, Campinas, SP, 2013. http://www.repositorio.unicamp.br/handle/REPOSIP/278193.

[22] S. Acharya et al. Transverse momentum spectra and nuclear modification factors of charged particles in pp, p-Pb and Pb-Pb collisions at the LHC, 2018.